Terahertz Near-Field Vortex Beams with Variable Intensity Profiles Based on Geometric Metasurfaces

Yang Zhu
University of Shanghai for Science and Technology
Yiwen Zhou
University of Shanghai for Science and Technology
Fuyong Yue
University of Shanghai for Science and Technology
Zhiyuan Fan
University of Shanghai for Science and Technology
Xiaofei Zang (xfzang@usst.edu.cn)
University of Shanghai for Science and Technology https://orcid.org/0000-0001-8557-895X
Yiming Zhu
University of Shanghai for Science and Technology
Songlin Zhuang
University of Shanghai for Science and Technology

Research Article

Keywords: Metasurfaces, Geometric phase, Generalized vortex, Near-field, Orbital angular momentum

Posted Date: March 21st, 2022

DOI: https://doi.org/10.21203/rs.3.rs-1447080/v1

Terahertz near-field vortex beams with variable intensity profiles based on geometric metasurfaces

Yang Zhu[1,#], Yiwen Zhou[1,#], Fuyong Yue[1], Zhiyuan Fan[1], Xiaofei Zang[1,2,*], Yiming Zhu[1,2,*], and Songlin Zhuang[1]

[1]*Terahertz Technology Innovation Research Institute, Terahertz Spectrum and Imaging Technology Cooperative Innovation Center, Shanghai Key Lab of Modern Optical System, University of shanghai for Science and Technology, Shanghai 200093, China.*

[2]*Shanghai Institute of Intelligent Science and Technology, Tongji University, 20092, China.*

[#]*These authors contributed equally to this work*

[*] *Correspondence: xfzang@usst.edu.cn; ymzhu@usst.edu.cn*

Abstract

Electromagnetic waves possessing orbital angular momentum, namely vortex beams, have attracted considerable attention in the fields ranging from optical communications to quantum science, due to their extraordinary information encoding capabilities. Vortex beams are traditionally exhibited with a donut-shaped intensity distribution, where a null intensity center surrounded by a bright ring, caused by the phase singularity. Here we propose and experimentally demonstrate geometric metasurface devices that can generate near-field vortex beams with variable intensity profiles. The generation of a vortex beam with tailored intensity profile is realized by integrating the azimuthal nonlinear phase and spiral phase into the ring-shaped anisotropic air-slit array. As proof-of-principle examples, multiple geometric metasurfaces that generate vortex beams with C_N-fold rotational symmetric or asymmetric intensity profile in the near-field are demonstrated in the terahertz domain. This unique capability for terahertz near-field vortex transmutation based on geometric metasurface approach opens an avenue to develop multifunctional integrated systems and system-on-chip devices, holding potential applications in microscopy, integrated photonics, quantum information processing and optical communication.

Keywords: Metasurfaces, Geometric phase, Generalized vortex, Near-field, Orbital angular momentum.

Introduction

Vortex beams carrying orbital angular momentum (OAM) naturally exhibit two typical characteristics: the helical/twisted wavefronts and doughnut-shaped intensity profiles [1, 2]. On one hand, the degree-of-freedom of helicity is dependent on the topological charge (l), which is originated from the azimuthal angle dependent phase profile defined as $\exp(il\varphi)$. Intrinsically, the OAM of electromagnetic (EM) waves has infinite number of eigen modes, which makes it a great candidate for applications of high-capacity data transmission and communication [3, 4]. Due to the special phase profile and the phase singularity, vortex beams have also been applied in particle manipulation and quantum exploration [5-7]. On the other hand, the traditional vortex beam is always exhibited with a doughnut-shaped intensity profile, that is a null intensity center surrounded by a bright ring with $O(2)$ continuous rotational symmetry. Indeed, when transforming the phase singularity with $O(2)$ continuous rotational symmetry into C_N-fold discrete rotational symmetry, vortex beams with variable intensity distributions can be generated [8-10]. Conventional approaches using the polygonal lenses or spatial light modulators as the diffractive elements have been proposed and demonstrated to generate vortex beams with the intensity profiles featuring C_N-fold discrete rotational symmetry. However, these traditional diffractive elements are limited to the bulk size and material dispersion, which inevitably degrades their system-on-chip (SOC) and integrating implementations.

Metasurfaces, also known as the two-dimensional metamaterials, provide an ultra-compact platform to precisely manipulate the properties of EM waves at will [11, 12]. Especially, geometric metasurfaces consisting of anisotropic meta-atoms with identical shape but different in-plane orientations are one of the well-studied metasurfaces, which can locally tailor the amplitude, phase and polarization of EM waves at subwavelength resolution [13]. By carefully designing the orientation of each anisotropic meta-atom, the required phase profile can be produced by a geometric metasurface, enabling the control of the wavefront of EM waves. Recent works regarding geometric metasurface such as generalized Snell's law [14-16], holograms [17-24], metalens [25-34], spin Hall effect [35-38], polarization convertors [39-43], and nonlinear photonics [44-47] have sufficiently proven its outstanding capabilities in EM wave manipulation. Moreover, the generations of vortex beams [48-52], vector vortex beams [53, 54] and perfect vortex beams [55-57] have been demonstrated using geometric metasurface approach. Recently, generalized vortex beams, in which the corresponding intensity profiles have C_N-fold discrete rotational symmetry instead of continuous rotational symmetry for conventional vortices, have been demonstrated in free space, because of unique properties in intensity and phase distribution, extending the study of vortex beam and providing a new perspective on controlling the properties

of EM waves. For example, Yang *et al*., [58] have designed geometric metasurfaces encoded with noncanonical vortex phase profile to realize the free-space optical vortex with variable intensity profile, and Zhang *et al*., [59] have developed metasurfaces for generating multiplexed vortex beams with generated intensity profiles. However, these previous studies focus on the vortex with variable intensity profile in the far field, and the intensity profiles of these generalized vortices are limited to the C_N-fold discrete rotational symmetry. Near-field vortices (or surface plasmonic vortices) generated by metal-based structures enable unprecedented capability in confining, manipulating and enhancing EM fields at subwavelength mode volumes, and thus, they open a new avenue to significantly reduce the vortex sizes that can be applied in integrated nanophotonics [60-62]. However, the near-field vortex transmutation, and in particularly, vortex with asymmetric intensity profile has not been well explored so far.

In this paper, we investigate the excitation of near-field THz (terahertz) OAM with variable intensity profiles based on geometric metasurfaces. Functionalities featuring of simultaneously generating near-field vortex beam and manipulating the corresponding intensity profile are realized by integrating the azimuthal nonlinear phase and spiral phase into geometric metasurfaces consisting of ring-shaped anisotropic slits with predesigned orientations. In experiment, we demonstrate the generation of near-field vortex beams with C_N-fold rotational symmetric, *i.e.*, C_3- C_4- and C_5-fold rotational symmetric, and asymmetric (*e.g.* vortex beam with arbitrary shape) intensity distributions using geometric metasurfaces encoded with the required phase profiles. The demonstrated metasurface approach for generating near-field THz vortex beams with variable intensity profile will enable various applications in manipulating particles, SOC, optical tweezers, to name a few.

Methodology

Figure 1 schematically shows a geometric metasurface that can transfer the incident THz waves (a Gaussian THz beam) into a near-field vortex with a predesigned topological charge and variable intensity profile. Such a geometric metasurface consists of air-slit arrays etched in an ultrathin gold film deposited on a polyimide (PI) substrate. By integrating a spiral phase and an extra azimuthal nonlinear phase into the geometric metasurface, the excited THz surface waves with a position-dependent phase from each air-slit can be formed into a vortex with variable intensity profile under the illumination of circularly polarized (CP) THz waves. The spiral phase is designed to convert the excited surface waves into a near-field vortex, while the azimuthal nonlinear phase enables the functionality in reshaping the corresponding intensity profile. By carefully designing the orientation of each air-slit, one can accurately control the topological charge and the intensity distribution of the near-field vortex.

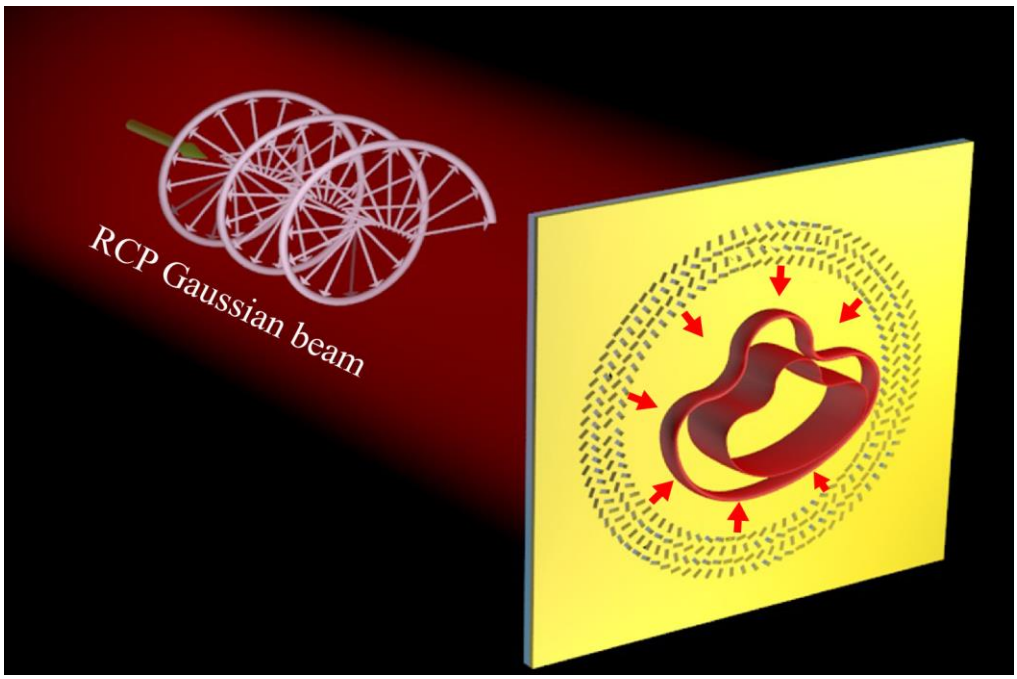

Fig. 1 Schematic of the geometric metasurface for generating near-field vortex with variable intensity profile: The ring-shaped geometric metasurface consists of air-slit arrays with predesigned orientations. For the incidence of RCP THz waves, the designed geometric metasurface allows to excite the surface waves into a near-field vortex with variable intensity profile.

The comparison of traditional vortex and generalized vortex with the corresponding phase structures are schematically shown in Fig. 2(a). For the traditional canonical vortex that contains a null intensity center surrounded by a bright ring due to the phase singularity (see inset of red curve in Fig. 2(a)), whereas the helical phase profile exhibits a linearly-increased phase in the azimuthal direction. While in terms of noncanonical/generalized vortex with variable intensity profile (see inset of the blue curve in Fig. 2(a)), an extra azimuthal nonlinear phase is added into the traditional spiral phase (a linearly-increased phase) to manipulate the intensity profile meanwhile preserving the topological charge. Since an anisotropic air-slit on a metal-based film can excite surface waves with tailored phase [63], the near-field vortex with nonlinear helical phase profile can be obtained by locally tailoring the orientation angle of each air-slit, as shown in Fig. 2(b). The optimized structure parameters of the ring-shaped metasurfaces are l=210 μm, w=60 μm, $\lambda_{SPP} = \lambda\sqrt{\frac{\varepsilon_d + \varepsilon_m}{\varepsilon_d \varepsilon_m}}$ (the wavelength of surface wave), $d=d_1=d_2\approx\lambda_{SPP}/2$, $\rho_0=m\lambda_{SPP}$ (m is integer, ρ_0 is the distance between the center of the air slit in the innermost ring and the origin of coordinates). The working wavelength of THz waves is $\lambda = 600$ μm. ε_m and ε_d are the permittivity of metal and dielectric, respectively.

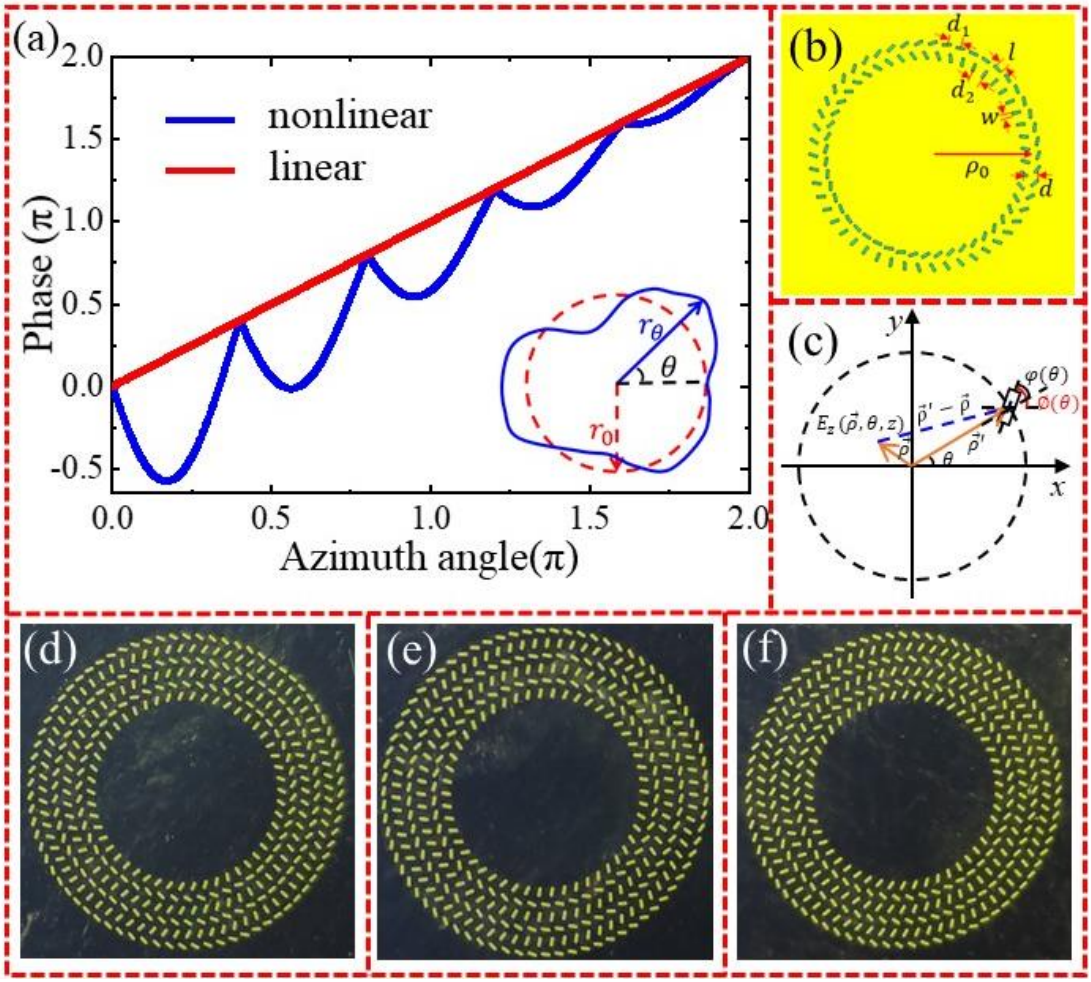

Fig. 2 The schematics of the fundament principle and the fabricated samples of the designed geometric metasurfaces. (a) The linear (red) and nonlinear vortex phase profiles along the azimuthal direction. (b) The designed structure of a geometric metasurface for generating near-field vortex with variable intensity profiles. (c) Schematic of an air-slit for exciting surface waves. (d-f) The optical images of the samples for respectively generating near-field vortices with C_3-, C_4-fold rotational symmetric, or asymmetric intensity profiles. Inset in (a) is the schematic of the vortices under the modulations of linear (red) and nonlinear vortex phase.

For an air-slit embedded in the gold film (see Fig. 2(c)), the excited surface waves under the illumination of CP EM waves can be expressed as:

$$E_z = e^{-\alpha z} A(\theta) e^{\pm i\phi(\theta)} e^{ik_{spp}|\vec{\rho}-\vec{\rho}'|}, \qquad (1)$$

where $A(\theta) = A_0 \cos(\varphi(\theta))$ is the amplitude of a dipole source and $\varphi(\theta) = \phi(\theta) - \theta$. $\pm$ is determined by the RCP and LCP incidence. ρ is the distance between field point and the origin of coordinates, while ρ' is distance between the center of each slit and the origin of coordinates. α is the attenuation coefficient.

When a single-ring structured air-slit array is designed, and each air-slit has a special rotation angle $\phi(\theta)$, the excited surface waves can be described as:

$$E_z = e^{-\alpha z}\int A(\theta)e^{\pm i\phi(\theta)}e^{ik_{spp}|\vec{\rho}-\vec{\rho}'|}d\theta, \tag{2}$$

To avoid the spin-assisted OAM number [64], a double-ring air-slit array (see Fig. 2(b)) with each unit cell containing a pair of orthogonally-distributed air-slits is employed to control the terahertz near-field OAM with variable intensity profiles. For the incidence of CP THz waves, the electric-field distribution for the double-ring air-slit array is governed as:

$$E_z = e^{-\alpha z}\int (A_{in}(\theta)e^{\pm i\phi(\theta)} + A_{out}(\theta)e^{\pm i(\phi(\theta)+\frac{\pi}{2})}e^{ik_{spp}d})e^{ik_{spp}|\vec{\rho}-\vec{\rho}'|}d\theta\cdot \tag{3}$$

Where d is distance between the inner and outer rings. If $\phi(\theta)=n\theta$ (a linearly-increased phase), then $A_{in}(\theta)=A_0\cos((n-1)\theta)$, $A_{out}(\theta)=A_0\cos((n-1)\theta+\frac{\pi}{2})$. When $d=\lambda_{SPP}/2$, the Eq.(3) can be rewritten as:

$$\begin{aligned} E_z &= e^{-\alpha z}\int (A_{in}(\theta)e^{\pm i\phi(\theta)} + A_{out}(\theta)e^{\pm i(\phi(\theta)+\frac{\pi}{2})}e^{ik_{spp}\frac{\lambda_{spp}}{2}})e^{ik_{spp}|\vec{\rho}-\vec{\rho}'|}d\theta \\ &= e^{-\alpha z}\int A_0(\cos(n-1)\theta \pm i\sin(n-1)\theta)e^{\pm in\theta}e^{ik_{spp}|\vec{\rho}-\vec{\rho}'|}d\theta \\ &= e^{-\alpha z}\int A_0 e^{\pm i(2n-1)\theta}e^{ik_{spp}|\vec{\rho}-\vec{\rho}'|}d\theta \\ &\propto J_{\pm(2n-1)}(k_{spp}\rho) \end{aligned}, \tag{4}$$

where J is the Bessel function. We set n=1, and thus, the topological charge of the generated near-field vortex (with a ring-shaped intensity profile) is ± 1. The initial rotation angles (at θ=0°) of the air slits in the inner and outer rings are $\pi/2$ and 0, respectively.

In order to generate a THz near-field vortex beam with variable intensity profile, a nonlinear phase should be introduced in the geometric metasurface:

$$\kappa(\theta)=\arg\left\{\exp[i\frac{2\pi}{\lambda_{spp}}((\vec{\rho}'\cos(\theta)-(r_\theta-r_0)\cos(\theta))^2+(\vec{\rho}'\sin(\theta)-(r_\theta-r_0)\sin(\theta))^2)]\right\}, \tag{5}$$

where r_0 is the constant that represents the radius of a traditional vortex and r_θ is the azimuthal-dependent radius of the vortex with variable intensity profile (see inset in

Fig. 2(a)). By embedding such nonlinear phase into our designed metasurface, the electric-field distribution in Eq.(4) is modulated as:

$$\begin{aligned} E_z &= e^{-\alpha z}\int (A_{in}(\theta)e^{\pm i(n\theta+\kappa(\theta))} + A_{out}(\theta)e^{\pm i(n\theta+\kappa(\theta)+\frac{\pi}{2})}e^{\pm in\kappa(\theta)}e^{ik_{spp}\frac{\lambda_{spp}}{2}})e^{ik_{spp}|\vec{\rho}-\vec{\rho}'|}d\theta \\ &= e^{-\alpha z}\int A_0(\cos(n-1)\theta \pm i\sin(n-1)\theta)e^{\pm in\theta}e^{\pm in\kappa(\theta)}e^{ik_{spp}|\vec{\rho}-\vec{\rho}'|}d\theta \\ &= e^{-\alpha z}\int A_0 e^{\pm i(2n-1)\theta}e^{\pm in\kappa(\theta)}e^{ik_{spp}|\vec{\rho}-\vec{\rho}'|}d\theta \\ &\propto J_{\pm(2n-1)}(k_{spp}\rho_\theta) \end{aligned} \tag{6}$$

Therefore, the rotation angles of the air slits in the inner and outer rings are $\phi_{inner}(\theta) = \kappa(\theta) + n\theta$ and $\phi_{outer}(\theta) = \kappa(\theta) + n\theta + \pi/2$, respectively.

For example, if breaking the traditional vortex with $O(2)$ continuous symmetry into C_N discrete rotational symmetry, the required structure parameter should be designed as:

$$r_\theta = \frac{r_0}{\cos(\frac{\pi}{N} - \mathrm{mod}(\theta, \frac{2\pi}{N}))}, \tag{7}$$

To obtain a near-field vortex with asymmetric intensity profile, the structure parameter can be written as:

$$r(\theta) = r_0\left\{1 + A(\theta)\sin\left[2\left(\theta - \frac{\pi}{4}\right)\right]\right\}, \tag{8}$$

where $A(\theta)$ is an azimuthal-dependent parameter and $A(\theta) \in [0,1]$.

Results and discussion

To verify the proposed method, we firstly design a geometric metasurface (see Fig. 2(d)) that can convert the incident THz waves into surface waves and simultaneously gather into a near-field vortex with C_3 discrete rotational symmetry propagating along the interface between air and metal, as shown in Fig. 3. The designed structure parameter for generating a near-field vortex with triangle-shaped intensity profile is set to be $r_\theta = r_0/(\cos(\frac{\pi}{3} - \mathrm{mod}(\theta, \frac{2\pi}{3})))$, where $\theta \in [0, \ 2\pi]$. The analytical electric field intensity ($|E_z|^2$) and phase distributions of the predesigned vortex are shown in Figs. 3(a_1) and 3(a_2), respectively. The vortex beam with a dark region in the center surrounded by a triangle-shaped intensity profile is observed, as shown in Fig. 3(a_1) (also see the black-dotted box). Such a non-canonical vortex is located at (0, 0), and the corresponding phase distribution (see the white-dotted box in Fig. 3(a_2)) also exhibits a triangle-shaped profile. There is only one phase jump from –π to π, indicating that a

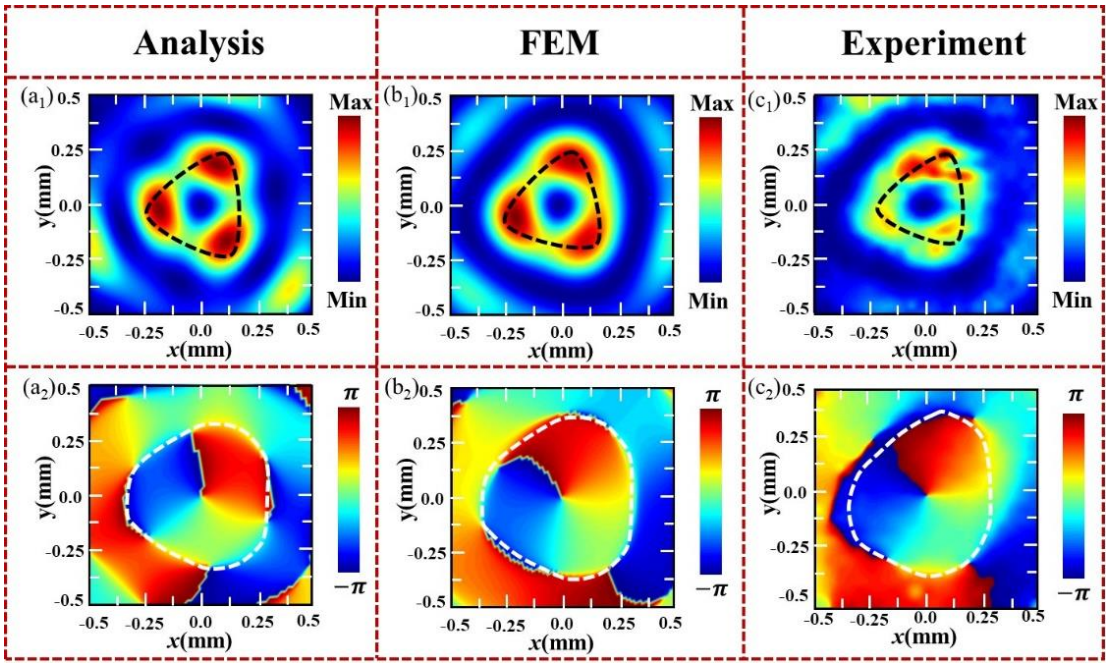

Fig. 3 The electric-field intensity ($|E_z|^2$) and phase distributions of the designed geometric metasurface encoded with C_3-fold rotational symmetric helical phase: (a_1) and (a_2) the analysis results, (b_1) and (b_2) the simulated results, (c_1) and (c_2) the measured results.

vortex beam with topological charge of +1 is preserved after the modulation of a triangle-shaped phase. Furthermore, by encoding such a singular phase (triangle-shaped phase) via accurately tailoring the orientation of each air-slit, such a near-field vortex with predesigned intensity profile can be realized (see both numerically simulated and experimentally measured results in Figs. 3(b_1)-3(c_2)). Finite element method (FEM) is used to numerically simulate the electric-field intensity and phase distributions of the resultant near-field vortex from metasurface. As can be seen from Fig. 3(b_1), under the illumination of right-handed circularly polarized (RCP) THz waves, the simulated electric field intensity distribution indeed exhibits a triangle-shaped hollow ring, demonstrating the symmetry breaking from $O(2)$ continuous symmetry into C_3-fold discrete rotational symmetry. The phase distribution shown in Fig. 3(b_2) also presents a triangle-shaped profile as expected. Experimentally, a near-field scanning THz time-domain spectrum microscopy system (see the experimental set-up in supplementary materials section 1) is used to characterize the performance of the fabricated metasurfaces. Figs. 3(c_1) and 3(c_2) illustrate the measured electric field intensity and phase distributions. A triangle-shaped vortex is observed nearby the surface of the fabricated sample, as shown in Fig. 3(c_1) (The distance between the detecting plane and the sample plane is about 100 μm). The measured intensity and phase in Fig. 3(c_1) and (c_2) shows a triangle-shaped profile, which agree well with the analysis and FEM results, except for a slight discrepancy that is attributed to imperfect quality of the input THz waves and the measurement errors.

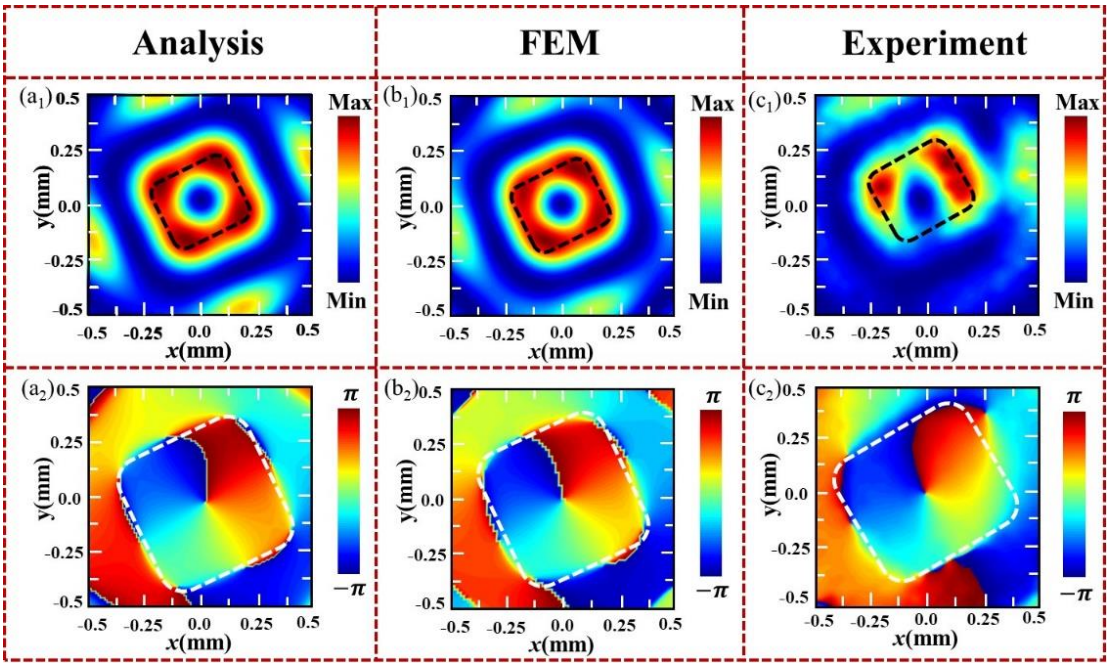

Fig 4. The electric-field intensity ($|E_z|^2$) and phase distributions of the designed geometric metasurface encoded with C_4-fold rotational symmetric helical phase: (a_1) and (a_2) the analysis results, (b_1) and (b_2) the simulated results, (c_1) and (c_2) the measured results.

To further demonstrate the versatility and robust of our proposed approach, the near-field vortex with C_4 discrete rotational symmetry is investigated, as shown in Fig. 4. Here, the designed structure parameter is designed as $r_\theta = r_0 / (\cos(\frac{\pi}{4} - \mathrm{mod}(\theta, \frac{\pi}{2})))$, where $\theta \in [0, \quad 2\pi]$. According to Eq. (3), the electric field intensity of such a vortex should be exhibited as a square-shaped profile. As can be seen in Fig. 4(a_1) for the analysis model, the generated vortex beam enables the C_4 discrete rotational symmetry, showing a dark zone in the center surrounded by a square-shaped bright ring. The phase distribution is shown in Fig. 4(a_2), which also exhibits a square-shaped profile (indicated by a white-dotted box). The topological charge of the resultant EM field is still l=1 for such a square-shaped vortex, since the phase change is 2π around the center. When such a phase profile (with C_4 discrete rotational symmetry) is embedded into a geometric metasurface by controlling the orientations of the air-slit array, the near-field vortex with square-shaped intensity profile can be generated, as shown in Figs. 4(b_1)-4(c_2). For the incidence of RCP THz waves, the calculated electric field intensity (see Fig. 4(b_1)) shows a square-shaped profile, and the corresponding phase distribution is also well matched with the intensity profile, exhibiting a square-shaped configuration. Figures 4(c_1) and 4(c_2) illustrate the measured electric-field intensity and phase distributions, respectively, exhibiting the expected square-shaped hollow and solid profiles and confirming the generation of excited vortex beam with C_4 discrete rotational symmetry. The further demonstration of a geometric metasurface that can

generate near-field vortex with C_5 discrete rotational symmetry is given in supplementary materials section 2.

The proposed method not only allows to convert the incident THz waves into surface waves with OAM and C_N-fold rotational symmetric intensity distribution, but also enables the functionality to steer THz beam into a near-field vortex with asymmetric intensity profile (see Fig. 5). The structure parameter for generating vortex with arbitrary intensity profile can be expressed as:

$$r_\theta = r_0\left\{1+A_\theta \sin\left[2\left(\theta-\frac{\pi}{4}\right)\right]\right\}, \tag{9}$$

where A_θ is variable along the azimuthal direction and $A_\theta \in (0,\ \ 1]$. As a proof-of-concept, the structure parameter is selected as:

$$r_\theta = \begin{cases} r_0\left\{1+0.3\sin\left[2\left(\theta-\dfrac{\pi}{4}\right)\right]\right\}, & \theta\in\left(\dfrac{\pi}{4},\dfrac{3\pi}{4}\right] \\ r_0\left\{1+0.5\sin\left[2\left(\theta-\dfrac{3\pi}{4}\right)\right]\right\}, & \theta\in\left(\dfrac{3\pi}{4},\dfrac{5\pi}{4}\right] \\ r_0 & ,\quad other \end{cases}. \tag{10}$$

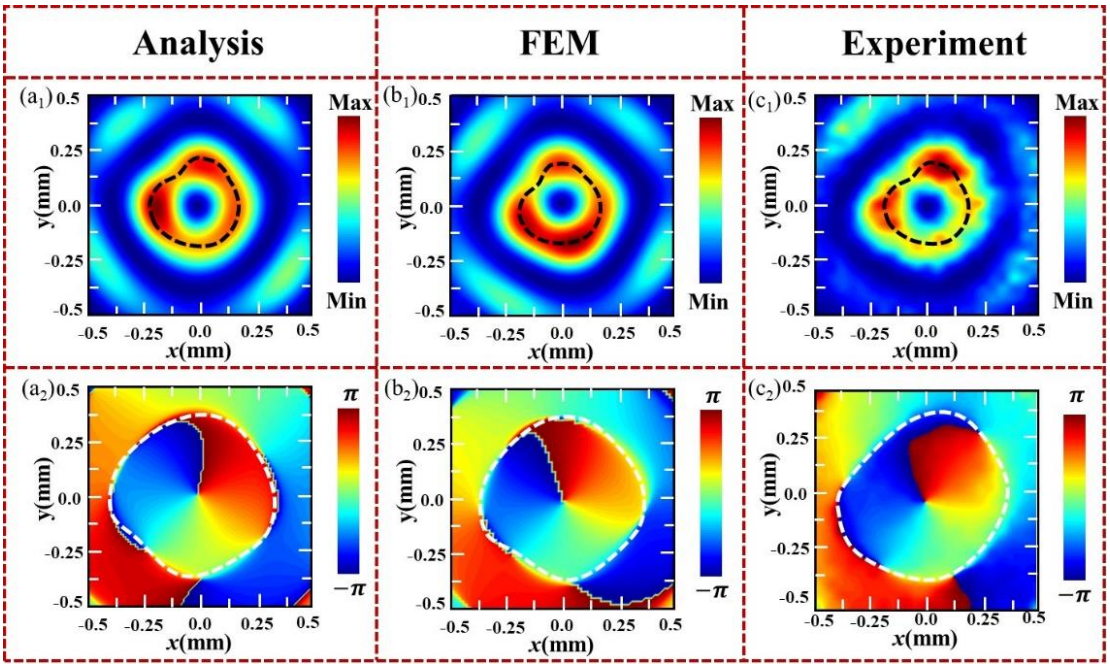

Fig 5. The electric-field intensity ($|E_z|^2$) and phase distributions of the designed geometric metasurface encoded with asymmetric helical phase: (a_1) and (a_2) the analysis results, (b_1) and (b_2) the simulated results, (c_1) and (c_2) the measured results.

According to Eq. (7), two different humps should be observed at azimuthal position of $\theta = \pi / 2$ and $\theta = \pi$ in the generated near-field vortex. Figures 5(a_1) and 5(a_2) illustrate the electric field intensity and phase distributions based on the analysis model. A vortex beam with one small hump at $\theta = \pi / 2$ and one large hump at $\theta = \pi$ is confirmed. Moreover, the corresponding phase distribution (indicated by the white box in Fig. 5(a_2)) presents two humps at $\theta = \pi / 2$ and $\theta = \pi$, respectively. The topological charge is still l=1, since the phase change in a round is 2π. Both the electric field intensity and phase distributions with two different humps demonstrate the asymmetric characteristic of the vortex beam. The simulated electric field intensity and phase profiles (see Figs. 5(b_1) and 5(b_2)) also show two dissimilar humps. The experimentally measured results of such a near-field vortex with asymmetric intensity profile are shown in Figs. 5(c_1) and 5(c_2). It is confirmed that both the measured electric field intensity (Fig. 5(c_1)) and phase (Fig. 5(c_2)) profiles exhibit the asymmetric characteristics. The measured results are well matched with the simulated and analysis results, indicating that our proposed approach can be extended to manipulate terahertz near-field OAM beam with arbitrary intensity profiles.

Conclusions

In conclusion, we have proposed and demonstrated a flexible approach to design air-slit-based geometric metasurfaces that could transfer the incident CP THz waves into surface waves possessing OAM and variable intensity profiles. The fundamental principle for simultaneously generating near-field vortex beam and manipulating the corresponding intensity profile was constructed by integrating the nonlinear azimuthal phase and spiral phase into the geometric metasurface design. By encoding the required phase profiles into a ring-shaped array that consists of anisotropic air-slits with specific local orientations, the near-field vortices with C_N-fold rotational symmetric and asymmetric intensity profiles were demonstrated. Our unique and flexible approach for simultaneously manipulating the near field OAM and the corresponding intensity profiles provides a unique capability to design multifunctional compact devices with potential applications in particle manipulation, information processing and system integration.

Methods

Sample fabrication

Traditional photolithography and magnetron sputtering coating were used to fabricate our designed THz near-field vortex generators. The PI (polyimide) film was selected as the substrate, and positive resist (AZP 4620) was spin-coated (4000 rpm, 30 s) on one side of the pre-cleaned substrate. Then, the mask was used for the exposure processing. After that, 150 nm gold was deposited based on the magnetron sputtering coating.

Finally, after the ultrasonic stripping, the metal-based metasurface array was formed. The experiment set-up for detecting the electric field intensity and phase distributions of the fabricated samples was given in supplementary materials section 1.

Abbreviations

OAM: orbital angular momentum; EM: electromagnetic; SOC: system-on-chip; PI: polyimide; CP: circularly polarized; THz: terahertz; RCP: right-handed circularly polarized; SPPs: surface plasmon polaritons.

Acknowledgments

Not applicable.

Funding

National Key Research and Development Program of China (2017YFA0701005), National Natural Science Foundation of China (61871268), "Shuguang" Program of Shanghai Education Commission (19SG44), the Key project supported by Science and Technology Commission Shanghai Municipality (YDZX20193100004960), Higher Education Discipline Innovation Project (D18014).

Authors' contributions

XFZ conceived the initial idea. YZ conducted the numerical simulations. YZ and YWZ performed the measurements. YZ and XFZ analyzed the data. All authors read and approved the final manuscript.

Availability of data and materials

The datasets used and analyzed during the current study are available from the corresponding author on reasonable request.

Declarations

Ethics approval and consent to participate

There is no ethics issue for this paper.

Consent for publication

All authors agreed to publish this paper.

Competing interest

The authors declare that they have no competing interests.

References

1. Allen L, Beijersbergen MW, Spreeuw RJ, Woerdman JP. Orbital angular momentum of light and the transformation of Laguerre-Gaussian laser modes. Phys. Rev. A. 1992; 45(11):8185-9.
2. Zhan Q. Cylindrical vector beams: from mathematical concepts to applications. Adv. Opt. Photonics. 2009; 1(1): 1-57.
3. Wang J, Yang JY, Fazal IM, Ahmed N, Yan Y, Huang H, et al. Terabit free-space data transmission employing orbital angular momentum multiplexing. Nat. Photonics. 2012; 6(7): 488-96.
4. Yan Y, Xie G, Lavery MPJ, Huang H, Ahmed N, Bao C, et al. High-capacity millimetre-wave communications with orbital angular momentum multiplexing. Nat. Commun. 2014; 5:4876.
5. Padgett M, Bowman R. Tweezers with a twist. Nat. Photonics. 2011; 5(6):343-8.
6. Chu J, Chu D, Smithwick Q. Encoding and multiplexing of 2D images with orbital angular momentum beams and the use for multiview color displays. Research. 2019; 2019: UNSP9564593.
7. Stav T, Faerman A, Maguid E, Oren D, Kleiner V, Hasman E, et al. Quantum entanglement of the spin and orbital angular momentum of photons using metamaterials. Science. 2018; 361(6407):1101-4.
8. Gao N, Xie CQ. Experimental demonstration of free-space optical vortex transmutation with polygonal lenses. Opt. Lett. 2012; 37(15):3255-7.
9. Hickmann JM, Fonseca EJS, Soares WC, Chávez-Cerda S. Unveiling a truncated optical lattice associated with a triangular aperture using light's orbital angular momentum. Phys. Rev. Lett. 2010; 105(5):053904.
10. Novoa D, Sola IJ, Garcıa-March MA, Ferrando A. The key role of off-axis singularities in free-space vortex transmutation. Appl. Phys. B. 2014; 116(4):779-83.
11. Yu NF, Genevet P, Kats MA, Aieta F, Tetienne JP, Capasso F, et al., Light propagation with phase discontinuities: generalized laws of reflection and refraction. Science. 2011; 334 (6054):333-7.
12. Huang LL, Chen XZ, Muhlenbernd H, Li GX, Bai BF, Tan QF, et al. Dispersionless phase discontinuities for controlling light propagation. Nano Lett. 2012; 12(11):5750-5.
13. Zang XF, Yao BS, Chen L, Xie JY, Guo XG, Balakin AV, et al., Metasurfaces for manipulating terahertz waves. Light: Adv. Manufacturing. 2012; 2:10.
14. Ni XJ, Emani NK, Kildishev AV, Boltasseva A, Shalaev VM. Broadband light bending with plasmonic nanoantennas. Science. 2012; 335(6067) 427.
15. Liu LX, Zhang XQ, Kenney M, Sun XQ, Xu NN, Ouyang CM, et al. Broadband metasurfaces with simultaneous control of phase and amplitude. Adv. Mater. 2015; 26(29):5031-6.
16. Liu ZC, Li ZC, Liu Z, Li JL, Cheng H, Yu P, et al. High-performance broadband circularly polarized beam deflector by mirror effect of multinanorod metasurfaces. Adv. Fun. Mater. 2015; 25(34):5428-34.
17. Ni XJ, Kildishev AV, Shalaev VM, Vladimir M. Metasurface holograms for visible light. Nat. Commun. 2013; 4(1):2807.
18. Yifat Y, Eitan M, Iluz Z, Hanein Y, Boag A, Scheuer J. Highly efficient and broadband wide-angle holography using patch-dipole nanoantenna reflectarrays. Nano Lett. 2014; 14 (5):2485-90.
19. Zheng G, Mühlenbernd H, Kenney M, Li GX, Zentgraf T, Zhang S. Metasurface holograms reaching 80% efficiency. Nat. Nanotechnol. 2015; 10(4), 30812 (2015).
20. Wen DD, Yue FY, Li GX, Zheng GX, Chan K, Chen S, et al. Helicity multiplexed broadband

metasurface holograms. Nat. Commun. 2015; 6(1):1-7.
21. Xu Q, Zhang XQ, Xu YH, Ouyang CM, Tian Z, Gu JQ, et al. Polarization-controlled surface plasmon holography. Laser Photonics Rev. 2017; 11(11):1600212.
22. Jin L, Dong Z, Mei S, Yu Y, Wei Z, Pan Z, et al. Noninterleaved metasurface for (2^6-1) spin- and wavelength-encoded holograms. Nano. Lett. 2018; 18(12):8016-24.
23. Wang Y, Guan YC, Li H, Ding X, Zhang K, Wang J, et al. Dual-polarized tri-Channel encrypted holography based on geometric phase metasurface. Adv. Photon. Res. 2020; 1(2):2000022.
24. Kim I, Jang J, Kim G, Lee J, Badloe T, Mun J, Rho J. "Pixelated bifunctional metasurface-driven dynamic vectorial holographic color prints for photonic security platform," Nat. Commun. 2021; 12:3614.
25. Chen XZ, Huang LL, Mühlenbernd H, Li GX, Bai BF, Tan Q, et al. Dual-polarity plasmonicmetalens for visible light. Nat. Commun. 2012; 3(1):1-6.
26. Chen XZ, Chen M, Mehmood MQ, Wen DD, Yue FY, Qiu CW, et al. Longitudinal multifocimetalens for circularly polarized light. Adv. Opt. Mater. 2015; 3(9):1201-6.
27. Arbabi A, Horie Y, Bagheri M, Faraon A. Dielectric Metasurfaces for complete control of phase and polarization with subwavelength spatial resolution and high transmission. Nat. Natechnol. 2015; 10(11):937-43.
28. Khorasaninejad M, Chen WT, Devlin RC, Oh J, Zhu AY, Capasso F. Metalenses at visible wavelengths: diffraction-limited focusing and subwavelength resolution imaging. Science. 2016; 352(6290):1190-4.
29. Lin RJ, Su VC, Wang S, Chen MK, Chung TL, Chen YH, et al. Achromatic metalens array for full-colour light-field imaging. Nat. Nanotechnol. 2018; 14(3):227-31.
30. Wang S, Wu P, Su V, Lai Y, Chen M, Kuo H, et al. A broadband achromatic metalens in the visible. Nat. Nanotechnol. 2018; 13(8):227-32.
31. Chen WT, Zhu AY, Sanjeev V, Khorasaninejad M, Shi ZJ, Lee E, et al. A broadband achromatic metalens for focusing and imaging in the visible. Nat. Nanotechnol. 2019; 13(3):220-6.
32. Zang XF, Ding HZ, Intaravanne Y. Chen L, Peng Y, Ke Q, et al. A multi-foci metalens with polarization-rotated focal points. Laser Photonics Rev. 2019; 13(12):1900182.
33. Zang XF, Xu WW, Gu M, Yao BS, Chen L, Peng Y, et al. Polarization-insensitive metalens with extended focal depth and longitudinal high-tolerance imaging. Adv. Opt. Mater. 2020; 8(2)**:**1901342.
34. Wang RX, Intaravanna Y, Li ST, Han J, Chen SM, Liu JL, et al. Metalens for generating a customized vectorial focal curve. Nano Lett. 2021; 21(5):2081-7.
35. Yin XB, Ye ZL, Rho J, Wang Y, Zhang X. Photonic Spin Hall Effect at Metasurfaces. Science, 2013; 339(6126):1405-7.
36. Ling XH, Zhou XX, Yi XN, Shu WX, Liu YC, Chen SZ, et al. Giant photonic spin Hall effect in momentum space in a structured metamaterial with spatially varying birefringence." Light Sci. Appl. 2015; 4(1):e290.
37. Luo WJ, Xiao SY, He Q, Sun SL, Zhou L. Photonic spin Hall effect with nearly 100% efficiency. Adv. Opt. Mater. 2015; 3(8):1102-8.
38. Zang XF, Yao BS, Li Z. Zhu Y, Xie JY, Chen L, et al. Geometric phase for multidinebsional manipulation of photonics spin Hall effect and helicity-dependent imaging. Nanophotonics, 2020; 9(6):1501-8.

39. Grady NK, Heyes JE, Chowdhury DR, Zeng Y, Reiten MT, Azad AK, et al. Terahertz metamaterials for linear polarization conversion and anomalous refraction. Science. 2013; 340(6183):1304-7.
40. Yu N, Aieta F, Genevet P, Kats MA, Gaburro Z, Capasso F. A broadband, background-free quarter-wave plate based on plasmonicmetasurfaces. Nano. Lett. 2012; 12(12):6328-33.
41. Fan R, Zhou Y, Ren X, Peng R, Jiang S, Xu D, et al. Freely tunable broadband polarization rotator for terahertz waves. Adv. Mater. 2015; 27(7):1201-6.
42. Zang XF, Gong HH, Li Z, Xie JY, Cheng QQ, Chen L, et al. Metasurface for multi-channel terahertz beam splitters and polarization rotators. Appl. Phys. Lett. 2018; 112(17):171111.
43. Wang S, Deng ZL, Wang YJ, Zhou QB, Wang XW, Cao YY, et al. Arbitrary polarization conversion dichroism metasurfaces for all-in-one full Poincaré sphere polarizers. Light Sci. Appl. 2021; 10: 24.
44. Li GX, Chen SM, Pholchai N, Reineke B, Wong PWH, Pun EYB, et al. Continuous control of the nonlinearity phase for harmonic generations. Nat. Mater. 2015; 14(6):607-12.
45. Almeida E, Bitto O, Prior Y. Nonlinear metamaterialss for holography. Nat. Commun. 2016; **7**(1):12533.
46. Walter F, Li GX, Meier C, Zhang S, Zentgraf T. Ultrathin Nonlinear metasurface for optical image encoding. Nano Lett. 2017; 17(5):3171-6.
47. Ma ML, Li Z, Liu WW, Tang CC, Li ZC, Cheng H, et al. Optical information multiplexing with nonlinear coding metasurfaces. Laser Photon. Rev. 2019; 13(7):1900045.
48. Yang YM, Wang WY, Moitra P, Kravchenko II, Briggs DP, Valentine J. Dielectric meta-reflectarray for broadband linear polarization conversion and optical vortex generation. Nano Lett. 2014; 14(3):1394-99.
49. Cheng H, Liu ZC, Chen SQ, Tian JG, "Emergent Functionality and Controllability in Few-Layer Metasurfaces." Adv. Mater. 2015; 27(36):5410-1.
50. Maguid E, Yulevich I, Veksler D, Kleiner V, Brongersma ML, Hasman E. Photonic spin-controlled multifunctional shared-aperture antenna array. Science 2016; 352(6290):1202-6.
51. Zang XF, Zhu YM, Mao CX, Xu WW, Ding HZ, Xie JY, et al. Manipulating terahertz plasmonic vortex based on geometric and dynamic phase. Adv. Opt. Mater. 2018; 7(3):1801328.
52. Zhang K, Yuan Y, Ding X, Li H, Ratni B, Wu Q, et al. Polarization-engineered noninterleaved metasurface for integer and fractional orbital angular momentum multiplexing. Laser Photon. Rev. 2020; 15(1):2000351.
53. Yue FY, Wen DD, Zhang CM, Gerardot BD, Wang W, Zhang S, et al. Multichannel polarization-controllable superpositions of orbital angular momentum states. Adv. Mater. 2017; 29(15):1603838.
54. Bao YJ, Ni JC, Qiu CW. A minimalist single-layer metasurface for arbitrary and full control of vector vortex beams. Adv. Mater. 2020; 32(6):1905659.
55. Han J, Intaravanne Y, Ma A, Wang R, Li S, Li Z, et al. Optical metasurfaces for generation and superposition of optical ring vortex beams. Laser Photon. Rev. 2020; 14(9):2000146.
56. Liu M, Huo P, Zhu W, Zhang C, Zhang S, Song M, et al. Broadband generation of perfect Poincaré beams via dielectric spin-multiplexed metasurface. Nat. Commun. 2021; 12(1):2230.
57. Xie J, Guo H, Zhuang SL, Hu JB. Polarization-controllable perfect vortex beam by a dielectric metasurface. Opt. Express. 2021; 29(3):3081-9.
58. Zhang YC, Gao J, Yang XD. Optical vortex transmutation with geometric metasurfaces of rotational symmetry breaking. Adv. Opt. Mater. 2019; 7(22):1901152.

59. Zhang X, Huang LL, Zhao RZ, Wei QS, Li X, Geng GZ, et al. Multiplexed generation of generalized vortex beams with on-demand intensity profiles based on metasurfaces. Laser Photon. Rev. 2022; 16:2100451.
60. Spektor G, Kilbane D, Mahro AK., Frank B, Ristok S, Gal L, et al. Revealing the subfemtosecond dynamics of orbital angular momentum in nanoplasmonic vortices. Science 2017; 355(6330): 1187−91.
61. Frank B, Kahl P, Podbiel D, Spektor G, Orenstein, M.; Fu L, Short-range surface plasmonics: localized electron emission dynamics from a 60-nm spot on an atomically flat single-crystalline gold surface. Sci. Adv. 2017; 3:700721.
62. Meng Y, Chen YZ, Lu LH, Ding YM, Cusano A, Fan AC, et al. Optical meta-waveguides for integrated photonics and beyond. Light Sci. Appl. 2021; 10:235.
63. Lin J, Mueller JB, Wang Q, Yuan G, Antoniou N, Yuan XC, et al. Polarization-controlled tunable directional coupling of surface plasmon polaritons. Science 2013; 340(6130):331−4.
64. Lee SY, Kim SJ, Kwon H, Lee B. Spin-direction control of high-order plasmonic vortex with double-ring distributed nanoslits. IEEE Photon. Technol. Lett. 2015; 27(7):705-8.

Supplementary Files

This is a list of supplementary files associated with this preprint. Click to download.

- PhotoniXSupplementarySub.docx